Virus Research 259 (2019) 90–96

Contents lists available at ScienceDirect

Virus Research

journal homepage: www.elsevier.com/locate/virusres

# Cryo-EM structure of native spherical subviral particles isolated from HBV carriers

Jianhao Cao[a,b,1], Junchang Zhang[c,g,1], Yanmeng Lu[d], Shuhong Luo[a,**], Jingqiang Zhang[e,**], Ping Zhu[b,f,*]

[a] Institute of Antibody Engineering, School of Laboratory Medicine and Biotechnology, Southern Medical University, 1023 South Shatai Road, Guangzhou, 510515, China
[b] National Laboratory of Biomacromolecules, CAS Center for Excellence in Biomacromolecules, Institute of Biophysics, Chinese Academy of Sciences, 15 Datun Road, Beijing, 100101, China
[c] Department of Liver Disease, Guangdong Hospital of Traditional Chinese Medicine (Zhuhai), 53 Jingle Road, Zhuhai, 519015, China
[d] Center of Electron Microscopy, Central Laboratory, Southern Medical University, 1023 South Shatai Road, Guangzhou, 510515, China
[e] State Key Laboratory of Biocontrol, School of Life sciences, Sun Yat-sen university, 135 Xingang Xi Road, Guangzhou, 510275, China
[f] College of Life Sciences, University of Chinese Academy of Sciences, Beijing, 100049, China
[g] Department of TCM, Shenzhen Hospital of Southern Medical University, 1333 Xinhu Road, Shenzhen, 518101, China

ARTICLE INFO

*Keywords:*
Hepatitis B virus
Surface antigen
Cryo-EM
3D reconstruction
Structural heterogeneity

ABSTRACT

Hepatitis B virus (HBV) contains 3 types of particles, i.e., 22-nm-diameter spherical and tubular subviral particles (SVPs) and 44-nm-diameter Dane particles. The SVPs are non-infectious and present strong immunogenicity, while Dane particles are infectious. In this study, we isolated spherical SVPs from HBV carriers' sera and determined their 3D structure at the resolution of ~30 Å by cryo-electron microscopy (cryo-EM) single-particle reconstruction. Our cryo-EM structure suggests that the native HBV spherical SVP is irregularly organized, where spike-like features are arranged in a crystalline-like pattern on the surface. Strikingly, the hepatitis B surface antigen (HBsAg) in the native spherical SVPs folds as protrusions on the surface, as those on the native tubular SVPs and Dane particles, but is largely different from that in the recombinant octahedral SVPs. These results suggest a universal folding shape of HBsAg on the native HBV viral and subviral particles.

## 1. Introduction

Hepatitis B virus (HBV) is the prototype member of *Hepadnaviridae* family. Its infection can cause both chronic and acute hepatitis, liver cirrhosis and hepatocellular carcinoma. It is estimated that near 250 millions people are infected with HBV and the number of deaths increases every year from chronic infection (Tillmann, 2007).

HBV is an enveloped virus which contains an icosahedral core surrounded by an outer lipid envelope. The HBV genome contains 4 overlapping open reading frames (ORFs), which are named S, C, P and X, respectively. The ORF S encodes 3 forms of hepatitis B surface antigen (HBsAg) with the same carboxyl-terminus but different starting amino-terminus. They are named small (S), middle (M) and large (L) HBsAg respectively. All forms of HBsAg are integrated proteins which are embedded in viral membrane with certain domains exposed to lumen or cytosol (Bruss, 2004). In HBV carriers, in addition to the infectious full HBV viral particles (Dane particles), a great number of non-infectious subviral particles (SVPs, spherical or tubular shape) are produced and secreted into the circulation. Both the envelope of Dane particles and the SVPs are mainly composed of HBsAg. In Dane particles, HBsAg can bind to the cell receptor and initiate the virus entry process. While the excessive production of SVPs can cause immune tolerance and contribute to the persistence of the chronic infection (Ganem and Prince, 2004). Both plasma-derived and yeast-derived recombinant HBsAg have been proved to be effective and efficient prophylactic vaccines against HBV (Hilleman, 2001, 2003; McAleer et al., 1984; Valenzuela et al., 1982).

To date, the structure of HBV capsid has been determined at atomic resolution (Wynne et al., 1999; Yu et al., 2013), but much less is known about the structure of HBsAg. Particularly, it remains to be addressed how HBsAg is organized in HBV virions, either in the envelope of Dane particles or in the form of SVPs. Previous studies revealed that the

* Corresponding author at: National Laboratory of Biomacromolecules, CAS Center for Excellence in Biomacromolecules, Institute of Biophysics, Chinese Academy of Sciences, 15 Datun Road, Beijing, 100101, China.
** Corresponding authors.
*E-mail addresses:* sluo815@gmail.com (S. Luo), lsszjq@mail.sysu.edu.cn (J. Zhang), zhup@ibp.ac.cn (P. Zhu).
[1] Contribute equally to the work.

https://doi.org/10.1016/j.virusres.2018.10.015
Received 22 June 2018; Received in revised form 19 October 2018; Accepted 19 October 2018
Available online 12 November 2018
0168-1702/ 

native tubular SVPs adopt a helical symmetry with spike-like features on the surface (Short et al., 2009), while the recombinant HBsAg SVPs expressed in transgenic mouse were found to have an octahedral symmetry (Gilbert et al., 2005). To our knowledge, there is no report on the structure of native spherical SVPs isolated from sera of HBV carriers.

In this study, we determined the 3D structures of native spherical SVPs isolated from HBV carriers' sera at a resolution of ~30 Å by cryo-EM single particle reconstruction. Our structures reveal obvious spike-like features arranged on the surface of native spherical SVPs with a crystalline-like pattern, which is very similar to that on the surface of native tubular SVPs (Short et al., 2009) and Dane particles (Dryden et al., 2006). These results suggest that HBsAg folds as protrusions on native HBV SVPs and Dane particles. Based on these structural features, we propose an assembly model of HBsAg in native HBV virions. In the model, the base of spike-like features is made of the carboxyl-terminus of HBsAg, while the amino-terminus of large HBsAg locates on the tip of the protrusion, which could help HBV bind to the receptor.

## 2. Material and methods

### 2.1. Purification of HBsAg particles

HBsAg-positive sera (HBV DNA > $10^7$) were collected in the Department of Laboratory in Guangdong hospital of Chinese traditional medicine (Zhuhai hospital). About 200 mL mixed sera from multi-individuals of HBV carriers were subjected to a low speed centrifugation (10,000×g) to remove undissolved substance. The supernatants were then pelleted at 109,000×g for 90 min using a SW40 rotor (Beckman, USA). Pellets were suspended in 1 mL Tris buffer (3 mM Tris 150 mM NaCl, pH 7.5) and further purified by centrifugation through a 10% to 40% (w/v) discontinuous gradient of sucrose density at 109,000×g for 60 min using the same rotor. The gradient was fractioned and diluted in Tris buffer up to 13.5 mL. Each fraction was then pelleted with ultra-centrifugation twice to remove the sucrose with the same centrifugation conditions as before and was finally suspended in 100 μL Tris buffer. Purified samples were stained with 1% ammonium molybdate and examined under FEI spirit G2 electron microscope (EM) operated at 120 kV.

### 2.2. Cryo-EM sample preparation and data acquisition

A Quantifoil EM grid (R2/2) was glow discharged and placed with an aliquot of 3 μL of purified SVPs. After that, it was blotted with a filter paper for 3–4 s in a chamber at 100% humidity and frozen in liquid ethane cooled by liquid nitrogen using an FEI Vitrobot. Data sets of cryo-EM were collected using serialEM software package (Mastronarde, 2003) under an FEI Talos F200C 200 kV electron microscope equipped with a DE20 direct electron detector (Direct Electron). The electron microscope was carefully aligned before the collection of micrographs. The range of defocus value was set to 1.5–2.5 μm. Micrographs were recorded with integration mode at a nominal magnification of 36,000×, corresponding to a pixel size of 1.25 Å. For each micrograph, an electron dose rate of 25e/Å$^2$/s was used with a total exposure time of 2 s for 32 frames. All frames were aligned and were used to yield a single micrograph. A total of 853 micrographs were collected.

### 2.3. Cryo-EM image processing and structure determination

A total of 37,571 particles were selected manually using e2boxer program in EMAN2 software package (Tang et al., 2007) and were then cut out from the micrographs using Relion2 (Kimanius et al., 2016; Scheres, 2012) with 2× binning. Contrast transfer function (CTF) parameters estimation was performed using Gctf (Zhang, 2016). The 2D and 3D classification and refinement were performed with Relion2.

The native SVPs appear highly heterogeneous (Fig. 1). To select the relatively homogeneous particles, we first performed two rounds of 2D classifications of all manually picked-up heterogenous particles on the raw data. Those particles in the classes with similar size and clear features were further picked up (19,905 particles in total) and were subsequently subjected to the 3D classification and reconstruction with an initial model of Gaussian ball as shown in Fig. S1. Finally, two maps were yielded for refinement and the reconstruction resolution was estimated based on gold-standard Fourier shell correlation (FSC) criteria (Scheres and Chen, 2012). Visualization of maps and structure comparison were performed on UCSF Chimera (Pettersen et al., 2004). The details of 3D reconstruction are described below.

### 2.4. Three dimensional reconstruction and validation

After two rounds of 2D classifications, the selected particles (19,905 particles in total) were subjected to 3D reconstruction (Fig. S1). To avoid model bias, we directly performed 3D classifications with an initial model of Gaussian ball without any symmetry imposed (C1 symmetry).

To testify how many types of particles or conformations may exist among the isolated native spherical SVPs, we performed a series of 3D classifications on the selected particles with different target number of classes, K, as defined in Relion (Scheres, 2012). In each round of 3D classification, every SVP particle was assigned into one of the classes and all particles were divided into K classes (Fig. S1). Those particles in the classes with obvious features were combined and subjected to the next round of 3D classification. In the first round of 3D classification, a target number of classes, i.e., K = 12, was set. A total number of 18,538 particles were selected from 5 classes and combined for the second round classification. In the second round of 3D classification, all other options were kept unchanged but the option K was reduced to 6. After the second round classification, 10,958 particles were selected from 4 classes and combined for the next step (Fig. S1). We then performed two parallel and independent third round of 3D classifications on those picked 10,958 particles with target number of classes K = 12 and K = 4 respectively. Strikingly, almost all of the particles were classified into only 3 classes (classes 1, 2, 3 in K = 4 job and classes 1, 8, 12 in K = 12 job, Fig. S1) in both jobs, and there are very few number of particles in other classes. That is, only three major classes or conformations are classified or identified in the native spherical SVPs, no matter how many classes are targeted to be divided. Interestingly, by comparing the particle members in each of the three classes of the two jobs (K = 4 and K = 12), a large number of particles were found to be grouped into the same class in both of the jobs. Specifically, most particles in class 3 of K = 4 job were grouped in class 1 and 8 of K = 12 job and most particles in class 12 of K = 12 job were grouped in class 1 and 2 of K = 4 job (Fig. S1, indicated by red and blue colors in round 3 classification). We then combined these common particles into 2 merged classes which represents two relatively homogeneous datasets, in which the repeated particles were removed. Then, 2 merged classes were subjected to further 3D classification independently, but no more classes were yielded. Finally, both two merged classes of picked particles were subjected to refinement and 3D reconstruction independently, and two final 3D maps were yielded.

## 3. Results and discussion

### 3.1. Purification and identification of HBV SVPs

We centrifuged about 200 mL HBV carriers' sera to pellet SVPs. The resulted pellets were suspended and passed through a sucrose density gradient (10%~40%) (See materials and methods for details). The negatively staining EM (NS-EM) analysis exhibited three kinds of distinctive particles, i.e., the 22nm-diameter spherical SVPs, tubular SVPs and the 44nm-diameter Dane particles (Fig. 1A), which is consistent with the previously reported morphology of HBV virions (Dane et al., 1970).

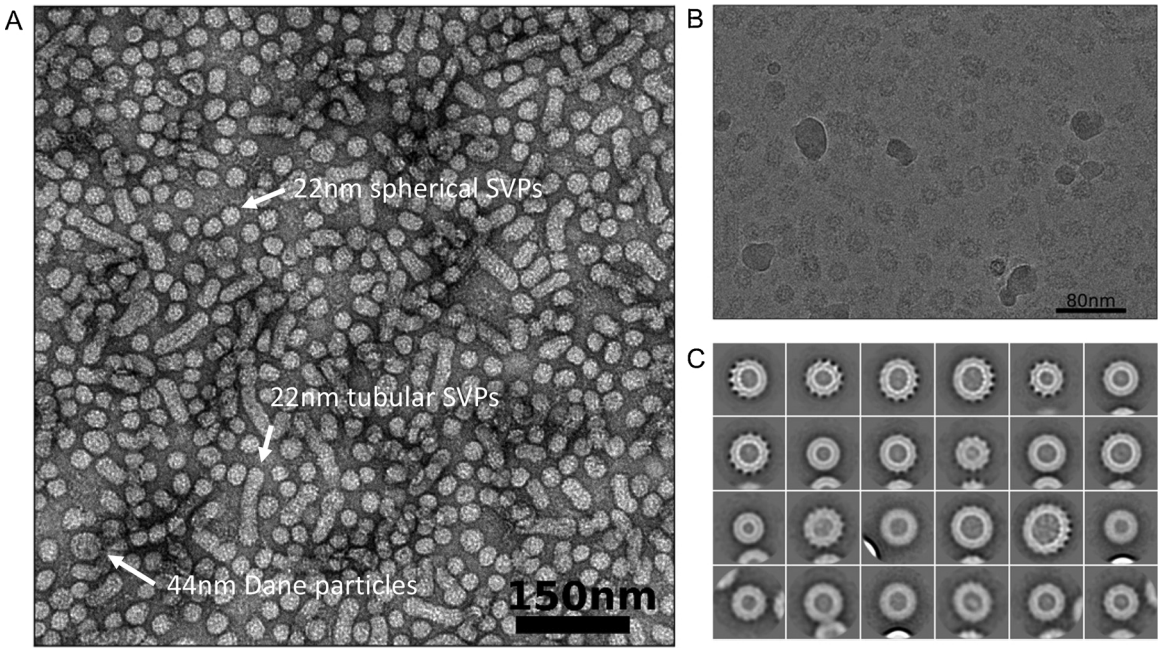


**Fig. 1.** Micrographs of HBV spherical SVPs. (A) Negative staining image of purified native spherical SVPs. All 3 types of HBV particles are indicated. (B) Cryo-EM image of purified native HBV SVPs. (C) Two-dimensional classification averaging images of spherical SVPs. Protruding features are readily visible around outer layers.

### *3.2. Structure determination of the native spherical SVPs*

To determine the structure of native HBV spherical SVP, we collected cryo-EM micrographs (Fig. 1B) of isolated spherical SVPs, and performed the data analysis and 3D reconstruction as described previously. The averaging images of 2D classification showed obvious protrusions around the surface of particles (Fig. 1C). Although the averaging images appear heterogeneous both in shape and in size (Fig. 1C), we managed to select a portion of relatively homogenous particles among them and performed the 3D reconstruction by single particle analysis (SPA) method (See Material and methods for details).

As described above in methods, during the third round of 3D classification, we noticed that almost all particles were clustered into only 3 classes, no matter the target number of classes (the option K) is set to 12 or 4 (Fig. S1). If we randomly split the data set into two halves and performed the 3D classification on the two data sets independently, the particles were found to be also grouped into 2 or 3 classes (Fig. S2). These 3D classification results suggest that the native spherical SVPs contain only a limited number of organization forms, and the structures of them can be determined by the SPA method. Our 3D reconstruction yielded two maps of native spherical HBsAg SVP with different sizes, 29.3 nm and 25.5 nm in diameter respectively (Fig. 2, Movie S1). The reconstruction resolutions for both maps are around 30.1 Å as determined by Fourier Shell Correlation (FSC) criteria at 0.143 cutoff (Fig. S3).

Both the two reconstruction maps show obvious spike-like features protruding from the surface (Fig. 2, Movie S1). This observation is similar to the previous ones on the native HBV tubular SVPs and Dane particles (Dryden et al., 2006; Short et al., 2009). But it is significantly different from that on the recombinant SVPs composed of only small HBsAg (Gilbert et al., 2005), which doesn't present any protrusion. In addition, no symmetry is globally presented in our maps, while the recombinant SVPs displays an octahedral symmetry (Gilbert et al., 2005).

In the cryo-EM density maps of the native spherical SVPs, spike-like features are locally arranged in a crystalline-like pattern (Fig. 2A). These protruding features are readily visible in the cryo-EM raw images (Fig. 1B and 3), averaged images of 2D classification (Fig. 1C and S4) and the re-projection images of the 3D maps (Fig. S4), although they are not fully decorated on the periphery of the particles (Fig. 1C and S4). Interestingly, the spike-like features on the native spherical SVPs are about 30 Å in height (Fig. 4B), which is 10 Å shorter than those on the tubular ones (Short et al., 2009) (Movie S2). It can also be directly observed in the cryo-EM raw images of different types of native HBV particles, i.e., spherical and tubular SVPs and Dane particles (Fig. 3). The average volume of protrusions (the parts outside the periphery of the SVPs) on tubular SVP was measured 75 $nm^3$ and that of spherical SVPs was measured 27 $nm^3$.

In the central sections of both density maps of spherical SVPs, we can clearly see the typical sandwich-like densities, which are highly likely attributed to the lipid bilayers (Fig. 2B). The thickness of this bilayer structure is around 50 Å, which is close to that of the membrane of vaccinia virus (50 Å) (Hollinshead et al., 1999) and that of influenza virus (60 Å) (Yamaguchi et al., 2008). The morphoresis of HBsAg components first takes place in the endoplasmic reticulum (ER) (Huovila et al., 1992; Patzer et al., 1986). And then the HBsAg-containing membrane buds as the envelope of Dane particles or SVPs. Both HBV Dane particles and SVPs contain lipid components which form the membrane (Gavilanes et al., 1982; Satoh et al., 1990). These results suggest that the bilayer structure in the reconstruction is attributable to the membrane of spherical SVPs. In addition, clear densities across the bilayers can be observed (Fig. 2B, indicated by white arrows). These densities are likely attributable to the transmembrane domains of the HBsAg peptides, which were also reported in tubular SVPs (Short et al., 2009). Interestingly, although the small native SVPs exhibit as spherical particles with variant diameters (Fig. 1), all of them present similar morphology on the surface, i.e., protrusions or spike-like features (Fig. 2).

Our cryo-EM reconstruction revealed that the spike-like features organize on the surface of spherical SVPs in a crystalline-like pattern, which is similar to the previous report on the structure of tubular SVPs (Short et al., 2009) (Fig. 4B, Movie S2). Interestingly, the HBsAg in Dane particles was also assembled on the surface of the virion with similar protrusions (Dryden et al., 2006). These results suggest that the HBsAg folds as a protrusion on the surface either in Dane particles or different SVPs, although they may organize in different ways.

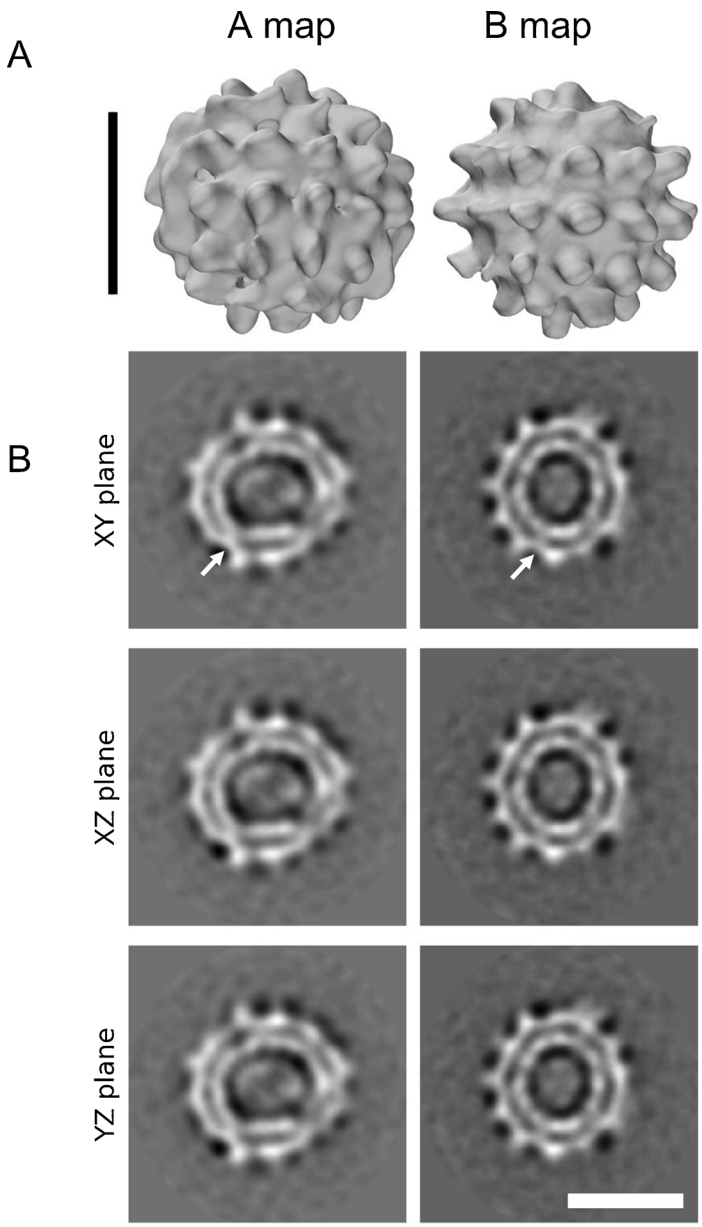


**Fig. 2.** Two cryo-EM 3D reconstruction maps of spherical SVPs. (A) Two reconstruction density maps of HBV spherical SVPs displayed as surface-rendering view. Both maps present spike-like features but with a slight difference in size. The diameter of A map is 29.3 nm, while that of B map is 25.5 nm. Scale bar is 20.0 nm. (B) Central sections of A map and B map from different planes perpendicular to each other. All of them show apparent lipid bilayers. White arrows indicate the presumptive densities crossing the lipid bilayers. Scale bar is 20.0 nm.

Nevertheless, all structural studies so far haven't achieved a high resolution structure of the HBsAg, suggesting a likely intrinsic heterogeneity, and a complicated organization of it.

### 3.3. Organization of HBsAg

In this study, we determined the cryo-EM structure of native spherical SVPs isolated from HBV carriers' sera. Two density maps had been acquired in our 3D classification and reconstruction (Fig. 2A, Movie S1). Both of the maps present obvious spike-like features on the periphery in a crystalline-like pattern, which is similar to those on tubular SVPs and Dane particles. Superposition of the two density maps of spherical SVPs shows that they display almost the identical height of spike-like features and similar distances between protrusions (Fig. 4A, Movie S1). We then compared the spike-like features between spherical and tubular SVPs. It is interesting that the height of spike-like features on spherical SVPs is 10 Å shorter than that on tubular ones, and the distance between protrusions on spherical SVPs (about 68 Å) is obviously less than that on tubular SVPs (about 116 Å) (Fig. 4B, Movie S2).

Three forms of HBsAg, i.e., S/M/L HBsAg, exhibit on the surface of HBV particles (Bruss, 2004). All of them have the same carboxyl-terminus but different amino-terminus, while the middle HBsAg has an extensive preS2 to the amino-terminus of small HBsAg (S region), and the large HBsAg has an extensive preS1 to the middle HBsAg (Fig. 4C). The volume of the protrusion on the tubular SVP is measured around 48 $nm^3$ larger than that on the spherical one (Fig. 4B, Movie S2). As the small HBsAg or the carboxyl-terminus of large/middle HBsAg forms the bottom of spike-like features integrated in the membrane, the extra volume of the protrusion on the tubular SVP is most likely contributed by the amino-terminus of large/middle HBsAg, i.e., preS1 and preS2 regions (Fig. 4C). Taken 1.25 $Å^3$/Da into consideration (Short et al., 2009), the volume difference (48 $nm^3$) of protrusions between the tubular SVP and the spherical one is caculated to be occupied by amino

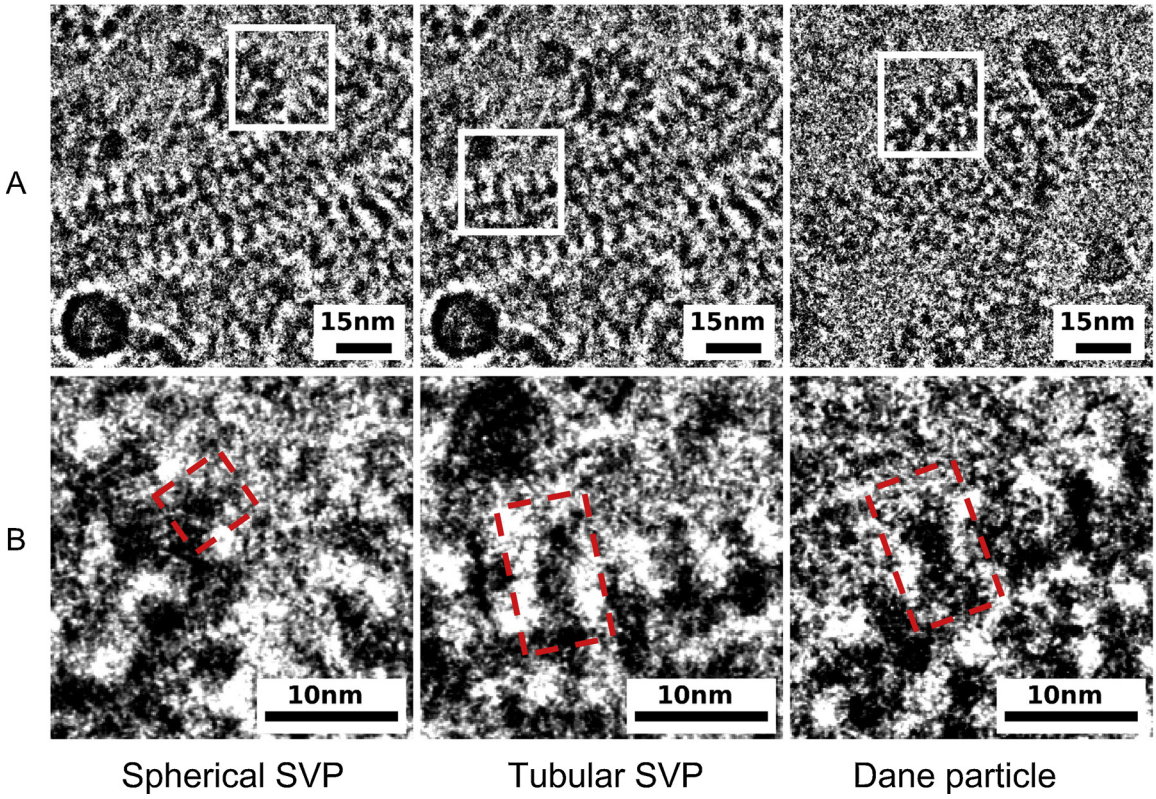


**Fig. 3.** Cryo electron micrographs of three 3 different forms of HBV viral particles. From left to right, Spherical SVP, Tubular SVP, Dane particle. (A) Cryo-EM micrographs show that the spike-like features exist on the periphery of all three types of HBV particles. (B) The zoom-in view of the boxed part in (A). Representative protrusions are indicated by red boxes and their size variance in different forms of particles are clearly visible (For interpretation of the references to colour in this figure legend, the reader is referred to the web version of this article).

acids (AAs) with molecular weight (MW) of ~38.4 KDa. The S/M/L HBsAg contains 226/281/400 AAs and the corresponding MW is about 25/31/44 kDa respectively, which gives rise to a ratio of ~9 A A/kDa. That means the extra volume in the protrusion of tubular SVP could hold ~350AAs which is about twice of the length of preS1 and preS2 domains (Fig. 4C). It suggests that a protrusion unit on the tubular SVP likely contains two large HBsAg components. In addition, the glycosylation in the preS1 or preS2 region of large HBsAg, such as P39 and GP42 (Heermann et al., 1984), could also contribute some extra densities to the protrusions of native tubular particles.

It has been well known that the HBsAg is integrated in the membrane and is the major component of HBV envelope. However, it has been reported that different types of HBV particles have variant stoichiometry of large, middle and small forms of HBsAg (Heermann et al., 1984). HBV Dane particles and tubular SVPs exhibit all of the 3 forms of HBsAg, while spherical SVPs contain almost only middle and small HBsAg (Heermann et al., 1984). Therefore, the size difference of spike-like features between spherical SVPs and tubular SVPs/Dane particles are likely due to the different proportion of S/M/L HBsAg components in these viral and sub viral particles, i.e., the higher stoichiometry of L/M HBsAgs, particularly the large HBsAg, contribute mostly to the higher protrusions in tubular SVPs/Dnae particles. The lack of large HBsAg on spherical SVPs makes its protrusions shorter than that on tubular SVPs. So as to the smaller distance between protrusions on spherical SVPs than that on tubular SVPs and Dane particles.

Based on these structural characteristics, we propose an assembly model of HBsAg on the surface of HBV Dane particles and SVPs (Fig. 4C). In this model, the S regions in S/M/L HBsAg fold in the same way with previously reported topology (Bruss, 2004), which could provide a structural base for protrusion units arranging regularly on membranes in a crystalline-like pattern as shown in both spherical SVPs (Fig. 2A) and tubular SVPs (Short et al., 2009). In HBsAg, only the S region contains transmembrane domains, so it most likely contributes to the regular arrangement of HBsAg on HBV membrane and determine the organization pattern of HBsAg in HBV virion. The central part of S region (AA99-169) folds as a luminal loop, which is the only domain of small HBsAg exposing outside and providing the general epitope (named “antigenic loop”) (Bruss, 2004). Subsequently, the short spike-like features in spherical SVPs likely contain only the antigenic loop and the preS2 region of middle HBsAg (Fig. 4C).

As previously reported, different HBV viral or sub viral particles exhibit variant proportion of S/M/L HBsAgs, while tubular SVPs and the envelope of Dane particles contain more large HBsAg than spherical SVPs (Heermann et al., 1984). Because the only difference between large HBsAg and middle/small HBsAg is the preS1 region, it suggests that the higher protrusions in tubular SVPs and Dane particles contain the additional preS1 region. Considering that myristylation and AA2-48 in preS1 region is essential for binding host receptors (Bruss et al., 1996; Gripon et al., 1995; Yan et al., 2012), we speculate that the extra 10 Å height density in spike-like features of tubular SVPs contains the preS1 region, which is spatially attached to the host receptor (Fig. 4C). Moreover, it will help the myristoyl group at the amino-terminus of HBsAg to anchor to the membrane of host cell.

## 4. Conclusion

In this study, we isolated native HBsAg spherical SVP from HBV carriers’ sera and determined its 3D cryo-EM structure. The structure shows that the spike-like protrusions on the native spherical HBsAg SVPs present similar morphology and distribution pattern to those on the native tubular HBsAg SVPs and the envelope of HBV Dane particles. The similar morphology and distribution pattern of HBsAg in native HBV Dane particles and SVPs suggests a universal folding mechanism of HBsAg. The different stoichiometry of S/M/L HBsAgs in variant HBV

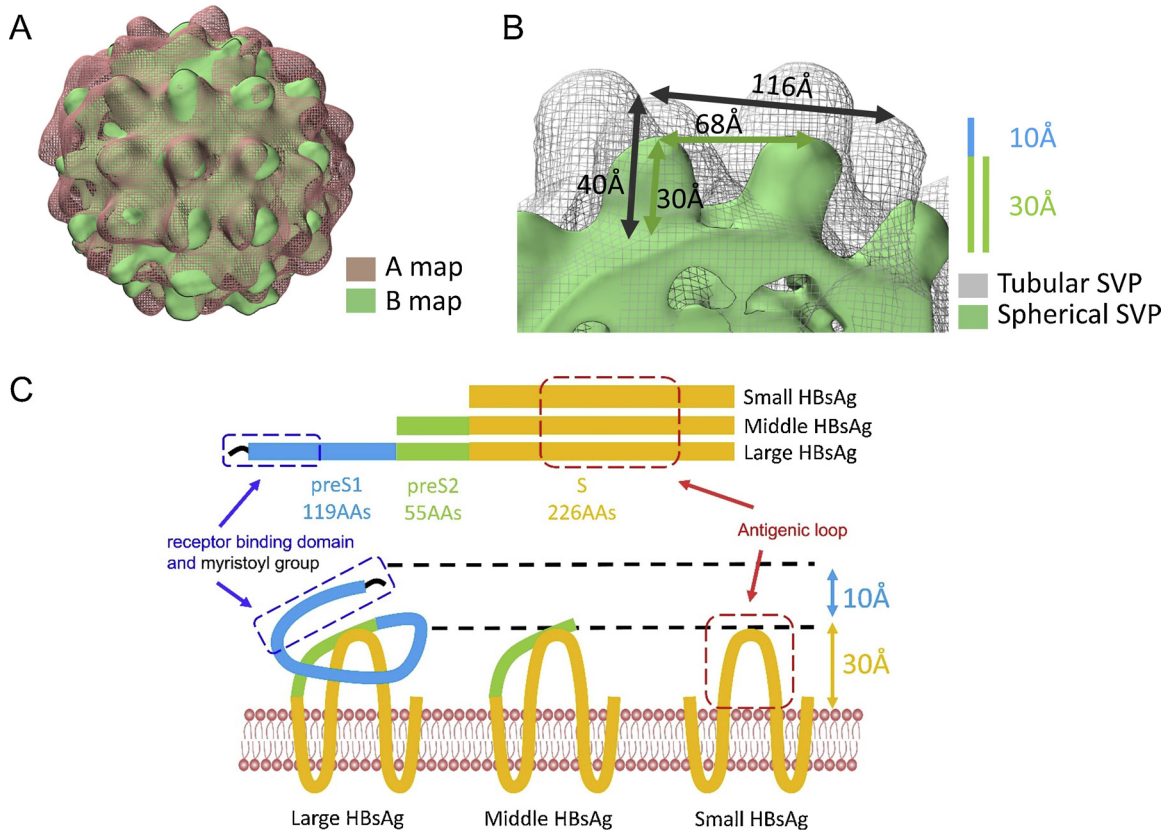


**Fig. 4.** Comparison of the density maps of spherical and tubular SVPs. (A) Superposition of two EM density maps of spherical SVP shows a slight difference in size, but the local spike-like features have almost identical arrangement. (B) Superposition of B map of spherical SVP and the map of tubular SVP(Short et al., 2009). The mesh map indicates the tubular SVP, while the solid map indicates the spherical SVP. The protrusions in spherical SVP are ~30 Å in height, about 10 Å shorter than that in tubular SVP. The distance between two tips of protrusions in spherical SVP is measured ~68 Å, apparently smaller than that in tubular SVP (~116 Å). (C) Illustration of S (yellow), preS2 (green), and preS1 (blue) domains in S/M/L HBsAg and an assembly model of the S/M/L HBsAg on the surface of HBV particles. Black line indicates the myristoyl group at the amino-terminus of large HBsAg. The preS1 (blue), preS2 (green), and S (yellow) regions are colored accordingly in the model. The exposed "antigenic loop" is indicated by a red dash line box, and the 50 amino acid residues in N-terminus of preS1 which involving in HBV functional receptor binding is indicated by a blue dash line box (For interpretation of the references to colour in this figure legend, the reader is referred to the web version of this article).

viral particles decide the size of spike-like features and the distance among them, which makes the appearance of HBsAg divergent in tubular or spherical SVPs, and in HBV virions.

To this date, most of the HBV vaccines contain only the small HBsAg peptides. The difference among the organization of S/M/L HBsAg may provide new spatial epitopes for development of prophylactic and therapeutic HBV vaccines.

## Accession numbers

The density maps of spherical SVPs have been deposited in the Electron Microscopy Data Bank with accession numbers EMD-6951 and EMD-6953 for A map and B map respectively.

## Conflict-of-interest statement

The authors declare that they have no competing interests.

## Funding statements

This work was supported by grants from the National Natural Science Foundation of China (31425007, 31730023 and 31521002), the National key research and development program of China (2017YFA0504700), and Strategic Priority Research Program (XDB08010100) from the Chinese Academy of Sciences.

## Acknowledgements

The EM and cryo-EM work was performed at the Center for Biological Imaging (CBI), Institute of Biophysics, Chinese Academy of Science (CAS). Computation of three-dimension reconstruction is performed at HPC-Service Station in Center for Biological Imaging, Institute of Biophysics, CAS.

We thank Dr. R. Anthony Crowther (MRC-LMB, UK) and Dr. Judith M. Short (MRC-LMB, UK) kindly provided the map of tubular SVP. We thank Dr. Hongrong Liu (Hunan Normal University, China), and Dr. Zheng Liu (Columbia University, USA) for critical comment and helpful discussion on this manuscript.

## Appendix A. Supplementary data

Supplementary material related to this article can be found, in the online version, at doi:https://doi.org/10.1016/j.virusres.2018.10.015.

## References

Bruss, V., 2004. Envelopment of the hepatitis B virus nucleocapsid. Virus Res. 106 (2), 199–209.

Bruss, V., Hagelstein, J., Gerhardt, E., Galle, P.R., 1996. Myristylation of the large surface protein is required for hepatitis B virusin VitroInfectivity. Virology 218 (2), 396–399.

Dane, D.S., Cameron, C.H., Briggs, M., 1970. Virus-like particles in serum of patients with Australia-antigen-associated hepatitis. Lancet 295 (7649), 695–698.

Dryden, K.A., Wieland, S.F., Whitten-Bauer, C., Gerin, J.L., Chisari, F.V., Yeager, M.,

2006. Native hepatitis B virions and capsids visualized by electron cryomicroscopy. Mol. Cell 22 (6), 843–850.
Ganem, D., Prince, A.M., 2004. Hepatitis B virus infection—natural history and clinical consequences. N. Engl. J. Med. 350 (11), 1118–1129.
Gavilanes, F., Gonzalez-Ros, J.M., Peterson, D.L., 1982. Structure of hepatitis B surface antigen. Characterization of the lipid components and their association with the viral proteins. J. Biol. Chem. 257 (13), 7770–7777.
Gilbert, R.J.C., Beales, L., Blond, D., Simon, M.N., Lin, B.Y., Chisari, F.V., Stuart, D.I., Rowlands, D.J., 2005. Hepatitis B small surface antigen particles are octahedral. Proc. Natl. Acad. Sci. U. S. A. 102 (41), 14783–14788.
Gripon, P., Le Seyec, J., Rumin, S., Guguen-Guillouzo, C., 1995. Myristylation of the hepatitis B virus large surface protein is essential for viral infectivity. Virology 213 (2), 292–299.
Heermann, K.H., Goldmann, U., Schwartz, W., Seyffarth, T., Baumgarten, H., Gerlich, W.H., 1984. Large surface proteins of hepatitis B virus containing the pre-s sequence. J. Virol. 52 (2), 396–402.
Hilleman, M.R., 2001. Overview of the pathogenesis, prophylaxis and therapeusis of viral hepatitis B, with focus on reduction to practical applications. Vaccine 19 (15), 1837–1848.
Hilleman, M.R., 2003. Critical overview and outlook: pathogenesis, prevention, and treatment of hepatitis and hepatocarcinoma caused by hepatitis B virus. Vaccine 21 (32), 4626–4649.
Hollinshead, M., Vanderplasschen, A., Smith, G.L., Vaux, D.J., 1999. Vaccinia virus intracellular mature virions contain only one lipid membrane. J. Virol. 73 (2), 1503–1517.
Huovila, A.P., Eder, A.M., Fuller, S.D., 1992. Hepatitis B surface antigen assembles in a post-ER, pre-Golgi compartment. J. Cell Biol. 118 (6), 1305–1320.
Kimanius, D., Forsberg, B.O., Scheres, S.H.W., Lindahl, E., 2016. Accelerated cryo-EM structure determination with parallelisation using GPUs in RELION-2. Elife 5 e18722.
Mastronarde, D.N., 2003. SerialEM: a program for automated tilt series acquisition on Tecnai microscopes using prediction of specimen position. Microsc. Microanal. 9 (S02), 1182–1183.
McAleer, W.J., Buynak, E.B., Maigetter, R.Z., Wampler, D.E., Miller, W.J., Hilleman, M.R., 1984. Human hepatitis B vaccine from recombinant yeast. Nature 307 (5947), 178–180.
Patzer, E.J., Nakamura, G.R., Simonsen, C.C., Levinson, A.D., Brands, R., 1986. Intracellular assembly and packaging of hepatitis B surface antigen particles occur in the endoplasmic reticulum. J. Virol. 58 (3), 884–892.
Pettersen, E.F., Goddard, T.D., Huang, C.C., Couch, G.S., Greenblatt, D.M., Meng, E.C., Ferrin, T.E., 2004. UCSF Chimera—a visualization system for exploratory research and analysis. J. Comput. Chem. 25 (13), 1605–1612.
Satoh, O., Umeda, M., Imai, H., Tunoo, H., Inoue, K., 1990. Lipid composition of hepatitis B virus surface antigen particles and the particle-producing human hepatoma cell lines. J. Lipid Res. 31 (7), 1293–1300.
Scheres, S.H.W., 2012. RELION: implementation of a Bayesian approach to cryo-EM structure determination. J. Struct. Biol. 180 (3), 519–530.
Scheres, S.H.W., Chen, S., 2012. Prevention of overfitting in cryo-EM structure determination. Nat. Methods 9 (9), 853.
Short, J.M., Chen, S., Roseman, A.M., Butler, P.J.G., Crowther, R.A., 2009. Structure of hepatitis B surface antigen from subviral tubes determined by electron cryomicroscopy. J. Mol. Biol. 390 (1), 135–141.
Tang, G., Peng, L., Baldwin, P.R., Mann, D.S., Jiang, W., Rees, I., Ludtke, S.J., 2007. EMAN2: an extensible image processing suite for electron microscopy. J. Struct. Biol. 157 (1), 38–46.
Tillmann, H.L., 2007. Antiviral therapy and resistance with hepatitis B virus infection. WJG 13 (1), 125.
Valenzuela, P., Medina, A., Rutter, W.J., Ammerer, G., Hall, B.D., 1982. Synthesis and assembly of hepatitis B virus surface antigen particles in yeast. Nature 298 (5872), 347–350.
Wynne, S.A., Crowther, R.A., Leslie, A.G.W., 1999. The crystal structure of the human hepatitis B virus capsid. Mol. Cell 3 (6), 771–780.
Yamaguchi, M., Danev, R., Nishiyama, K., Sugawara, K., Nagayama, K., 2008. Zernike phase contrast electron microscopy of ice-embedded influenza A virus. J. Struct. Biol. 162 (2), 271–276.
Yan, H., Zhong, G., Xu, G., He, W., Jing, Z., Gao, Z., Huang, Y., Qi, Y., Peng, B., Wang, H., 2012. Sodium taurocholate cotransporting polypeptide is a functional receptor for human hepatitis B and D virus. elife 1 e00049.
Yu, X., Jin, L., Jih, J., Shih, C., Zhou, Z.H., 2013. 3.5 Å cryoEM structure of hepatitis B virus core assembled from full-length core protein. PLoS One 8 (9) e69729.
Zhang, K., 2016. Gctf: real-time CTF determination and correction. J. Struct. Biol. 193 (1), 1–12.